

Review

# Fatigue of Thin, Oligo-Crystalline Wires Made of X2 CrNiMo 18-15-3

Bojan Mitevski <sup>1,2,\*</sup> and Sabine Weiß <sup>2</sup> 

<sup>1</sup> ITM, Materials Science & Engineering, University of Duisburg-Essen, Lotharstr. 1, 47057 Duisburg, Germany

<sup>2</sup> BTU Cottbus-Senftenberg, Chair of Physical Metallurgy and Materials Technology, Konrad-Wachsmann-Allee 17, 03046 Cottbus, Germany; sabine.weiss@b-tu.de

\* Correspondence: bojan.mitevski@uni-due.de; Tel.: +49-203-379-1266

Received: 31 March 2018; Accepted: 7 May 2018; Published: 9 May 2018



**Abstract:** For a variety of applications, such as in miniaturized machines, tools for minimal invasive surgery, or coronary stents, microscale components are used. For all these components, their dimensions are far below the size of conventional test specimens, and thus the grain size can approach the dimension of the cross section in these microscale components. According to experimental results, large differences in the mechanical behavior of the material occur between single- and polycrystalline test specimens. Therefore, oligo-crystalline microstructures are defined as a transition between single- and polycrystal. To investigate and understand the fundamental impact of oligo-crystalline microstructures on the mechanical behavior of the material, thin wires made of the austenitic CrNiMo steel 316LVM were fatigued. The choice of the material is justified, because it is one of the most frequently-used materials for coronary stents, and only a small amount of research has been done on oligo-crystalline microstructures of this material. Solution were annealed and 10% cold drawn oligo-crystalline wires were compared. The cold drawn wires exhibit an endurance limit of 450 MPa, which is significantly higher compared to solution annealed oligo-crystalline wires (250 MPa). Electron backscattering diffraction (EBSD) measurements of the fatigued wires show massive grain rotations, which lead to orientation changes within the grains. Sometimes, the deformation of a whole structure is concentrated on just one or only very few grains, with a particularly high Schmid factor (>0.44).

**Keywords:** oligo-crystalline microstructure; orientation mapping; wires; coronary stents; strut thickness

## 1. Introduction

The CrNiMo-steel type 316LVM (DIN EN 1.4441) is one of the most used metals for coronary stents [1,2]. Its austenitic microstructure provides good properties for ductility and strength [3,4]. A minimized stent strut thickness is important for the successful application of stents. Clinical studies revealed a significantly lower risk for early and late in-stent restenosis for thin-strut stents compared to stents with thick struts [1,5–8].

In addition to clinical studies, up to now, only a small amount of research has been done on the mechanical properties of oligo-crystalline components. Corresponding computer simulations reveal that the properties of these oligo-crystals can neither be considered as single-, nor as poly, crystalline behavior [9,10]. Additionally, in previous studies, authors have shown strongly deviating monotone mechanical properties of thin wires, depending on the local crystallographic grain orientation [11,12]. In tensile tests, the oligo-crystalline wires showed a strongly varying, 40–80% lower elongation at fracture compared to the one of wires with a polycrystalline microstructure [12]. The values of yield and tensile strength of oligo-crystalline wires are almost half when compared to those of polycrystalline wires, with high deviation, respectively [12]. In the literature, the term “size effect” is often used as

a reason for the deviating properties of thin, compared to thick, components. In most cases this is referred to as a geometrical thin, but still polycrystalline, structures. Size effects and oligo-crystalline microstructures in stainless steels, tantalum, nickel alloys, aluminum, titanium alloys and copper have been investigated in several studies [3,4,13–25] in relation to monotone and cyclic mechanical properties. Within this study, the properties of oligo-crystalline thin wires in solution annealed and a cold drawn state (such as in the case of stents, before and after dilatation) will be compared. Both states are relevant in the case of stents. The expansion or dilatation of a stent within the human body causes an irreversible cold drawing. For polycrystalline 316LVM, Goebbler [26] found an improvement in endurance limit, from 260 MPa in solution annealed condition to 400 MPa in a cold drawn state, which shall also be investigated for oligo-crystalline 316LVM in this study. Initially, stress-strain curves were also conducted to prove the monotone behavior of both wire conditions.

## 2. Materials and Methods

Commercially available hard-drawn wires with a diameter of 0.5 mm, made of 316LVM (for chemical composition see Table 1) were used. The wires were annealed at 1050 °C for 160 s by means of a conductive heat treatment set-up (Figure 1a,b). To prevent oxidation, a glass tube was flooded with argon for 10 s prior to the start of heat treatment and was stopped 10 s after heat treatment, when the wire was visibly cooled down. The argon flows into the upper part of the glass tube and heats up while falling to the lower part of the tube with a consequent loss of wire cooling. The temperature gradient within the annealing set-up was controlled pyrometrically. After coarse grain tempering, the lower third (35 mm part) of the heat-treated wire (region of highest temperature) was used for further preparation and mechanical tests.

**Table 1.** Chemical composition (wt-%) of the used 316LVM (X2 CrNiMo 18-15-3/DIN EN 1.4441) wire (Ø 0.5 mm).

Fe	C	Cr	Cu	Mn	Mo	N	Ni	P	S	Si
balanced	0.030	18.100	<0.500	1.300	2.800	0.04	14.0	0.020	0.005	0.400

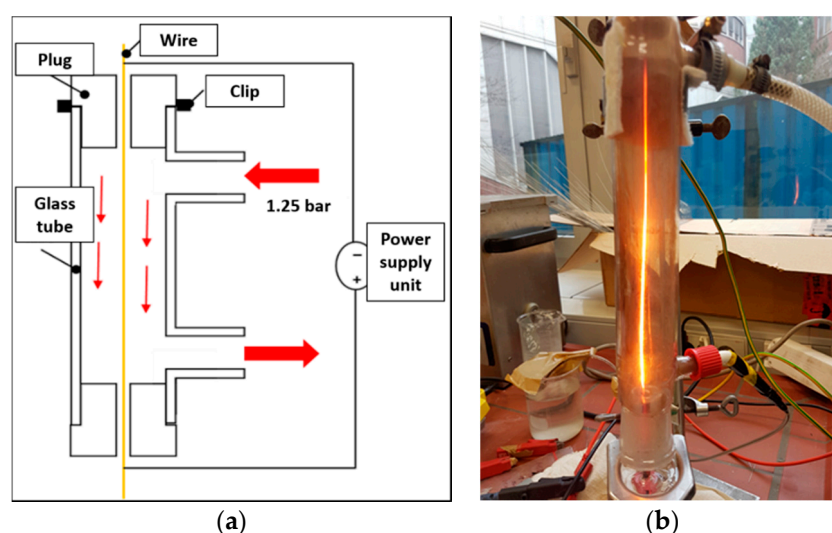


**Figure 1.** (a) Conductive heat treatment set-up scheme and (b) during heat treatment.

In the following step, the cut out, 35-mm parts were electro-polished with constant current settings (6 V; 0.45 A) for 20 s. Electro-polishing was conducted in an electrolyte containing 11 parts sulfuric acid (85%) and 7 parts phosphoric acid (96%) to achieve a minimal surface roughness after the heat treatment, where minimal oxidation on the wire surface could occur. Prior to the fatigue test, a group

of 23 wires was drawn for 10% of the reference length (20 mm) within a micro tensile testing device from Kammrath and Weiss (Dortmund, Germany), with special clampings for round wires. Drawing and the initial tensile tests were realized with a drawing speed of 10  $\mu\text{m/s}$ . A group of 36 wires was tested without previous additional drawing.

For the fatigue tests, two pneumatic test systems ((1) MTS Tytron™ 250, MTS Systems Corp., Eden Prairie, MN, USA and (2) DHM Prüfsystem, Clausthal-Zellerfeld, Germany) with the same clamping type were used (Figure 2a,b). To prevent buckling, the tests were carried out using a stress ratio of  $R = 0.5$ . A frequency of 7 Hz was a compromise between the test duration and the possible heating of the wire at high frequencies. Thin wires can dissipate the resulting heat better than thick specimens due to the advantageous relation of surface to volume of the wire. For both machines, 7 Hz was the highest possible frequency where machine control could apply a clean sinus signal on the wire specimens. All fatigue tests were performed at ambient temperature ( $20 \pm 1$  °C).

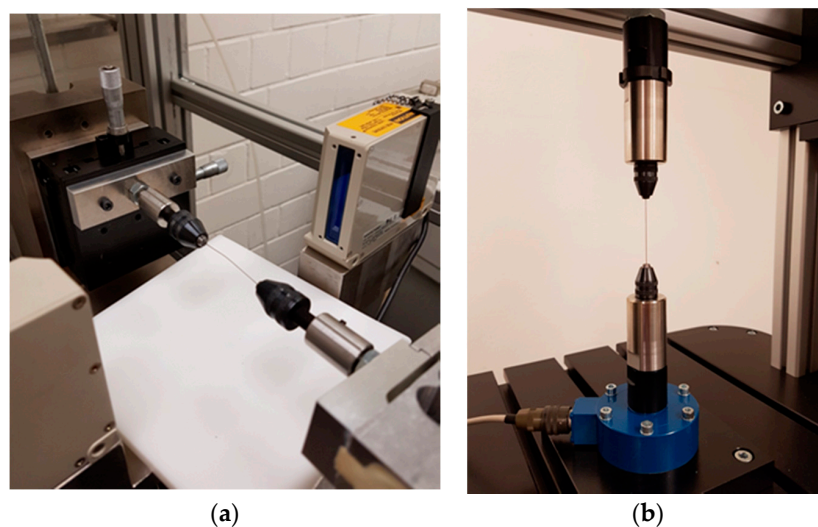


**Figure 2.** Pneumatic test system for fatigue tests: (a) MTS Tytron™ 250 and (b) DHM.

Either after fracture or when two million load cycles were completed, the test was stopped automatically. Fracture normally happens during stress increases. After fracture, the clampings were kept in their current positions to avoid a contact between the fracture surfaces. In the case of no fracture, the force was automatically, slowly decreased to 0 N to prevent further load, before the specimen could be removed.

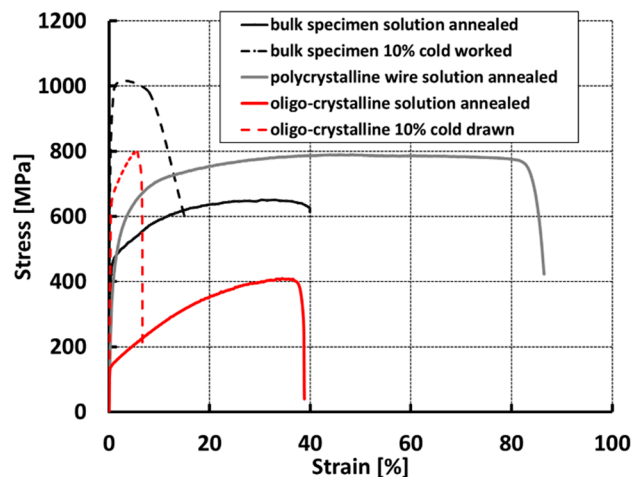
To perform EBSD, a representative number of fractured and non-fractured wires were mechanically ground (P1200) and polished (0.05  $\mu\text{m}/\text{SiO}_2$ ) parallel to the longitudinal axis of the wire until the mid-section was reached. Subsequently, the wires were electro-chemically polished for 20 s with the same electrolyte and parameters as those used before (6 V; 0.45 A). The microstructure was investigated by means of electron backscatter diffraction (EBSD) (AMETEK-EDAX, Ametek GmbH, Wiesbaden, Germany) with the corresponding software “OIM data collection” as well as “OIM data analysis”. An accelerating voltage of 20 kV and a 120- $\mu\text{m}$  aperture inside a Leo Gemini 1530 scanning electron microscope (Carl Zeiss Microscopy GmbH, Munich, Germany) was used.

### 3. Results and Discussion

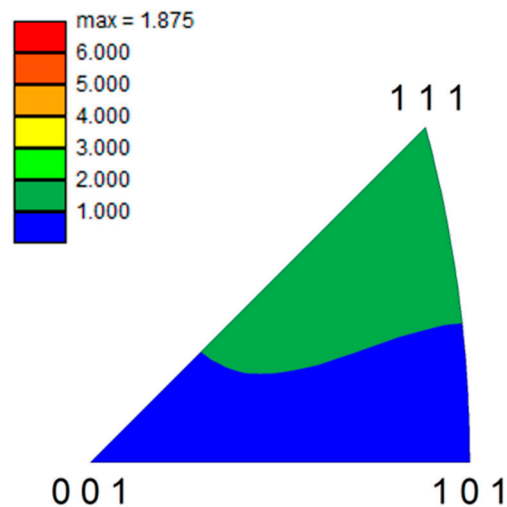
#### 3.1. Monotone Mechanical Properties of Oligo-Crystalline Wires

Figure 3a shows the stress–strain curves of the two considered wire conditions (solution annealed and 10% cold drawn) with respect to 316LVM bulk specimens (taken from Referene [26]), and a polycrystalline wire from of a previous study by the authors [12]. The cold drawing of the wires

increased the tensile strength from an average of 415 MPa to 804 MPa and decreased the fracture strain from 38% to 8%. A similar behavior could be observed for (polycrystalline) bulk specimens, tested by Goebbler [26]. He justifies this behavior with the generation of dislocations and a {111}-texture through cold working, which is also transferable to oligo-crystalline wires. Therefore, the inverse pole figure texture map in Figure 3b shows the crystallographic orientation distribution of a 10% cold worked wire before testing—a weak {111}-texture is visible. Furthermore, oligo-crystalline wires show a substantially lower strength and fracture strain compared to polycrystalline (wire) specimens. This is related to the low amount of grain boundaries in oligo-crystalline specimens and to the rotation of the grains' slip planes towards the direction of maximum slip, which can lead to an early fracture.



(a)



(b)

**Figure 3.** (a) Stress–strain curves of oligo-crystalline solution annealed and 10% cold drawn wires in relation to polycrystalline 316LVM bulk specimens (taken from Goebbler [26]) and (b) inverse pole figure (IPF) texture map for an oligo-crystalline 10% cold drawn wire before testing.

### 3.2. Cyclic Mechanical Properties of Oligo-Crystalline Wires

In Figure 4, Woehler diagrams of the fatigue tests on solution annealed and 10% cold drawn wires are shown. As expected, the maximum stress is significantly higher for the cold drawn wires than for the solution annealed ones. The solution annealed wires show high deviations in the number of

cycles to failure ( $N_f$ ). At different load levels, between 275 MPa and 350 MPa, the number of cycles to failure ranged between the very first cycle and two million cycles. An overshooting or significant undershooting of the machine control could be excluded.

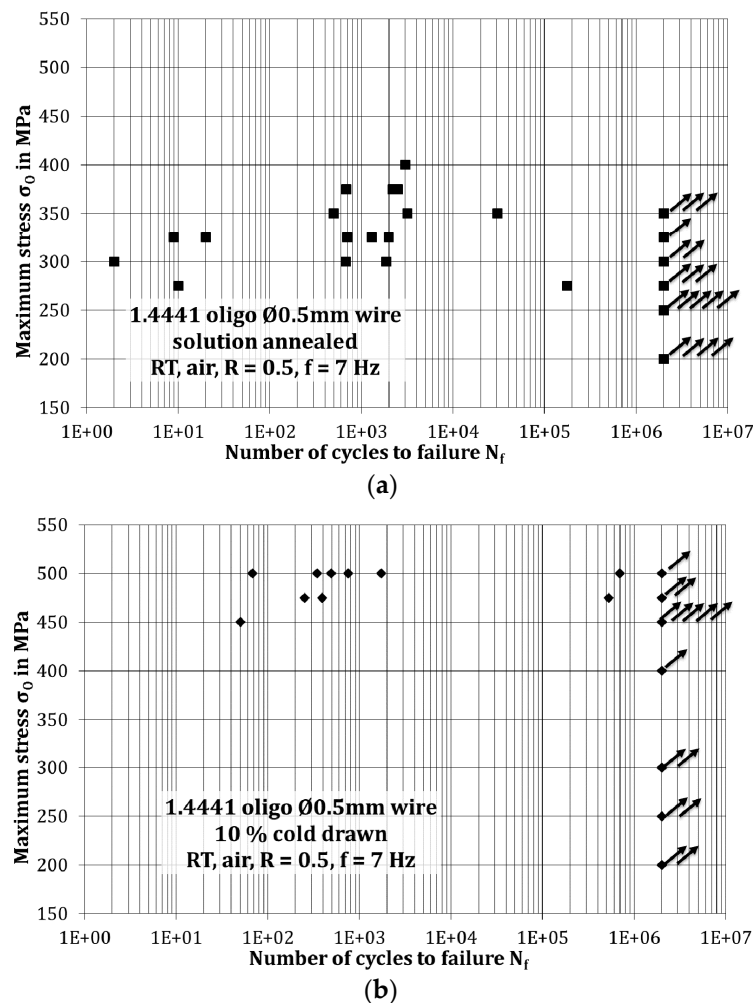
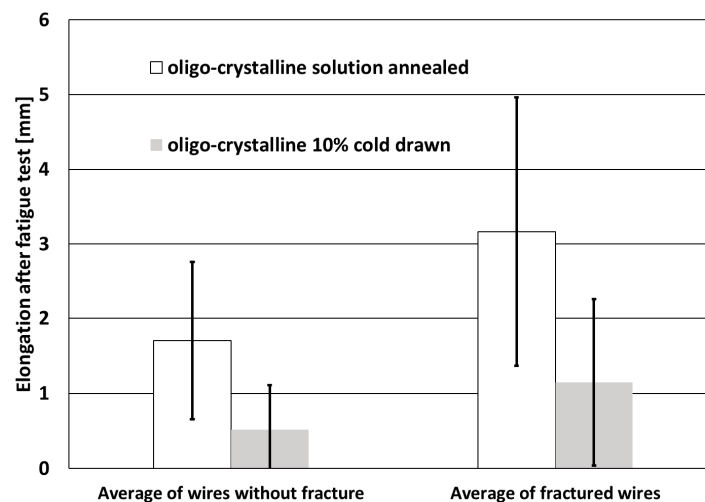


Figure 4. Woehler diagrams of (a) solution annealed and (b) 10% cold drawn 316LVM wires.

With respect to the high deviations, the endurance limit was defined as when a minimum of five wires on a specific load level reached two million cycles. Accordingly, the endurance limit was determined at 250 MPa. Donnelly [16] found in his work, with 50, 75, 100 and 150  $\mu\text{m}$  thick struts, laser cut from a 316L tube, a high deviation in the number of cycles to failure. The occurrence of fatigue-tested specimens without rupture of the thicker struts (on a higher level than for thinner struts) increased with increasing strut thickness, but with the low number of fatigue-tested specimen without rupture, an endurance limit could only be estimated at a higher level, but not ensured. Because of different key parameters, the values of the current study and the ones of Donnelly's work (500–600 MPa [18]) are difficult to compare. The higher strength of the thin struts in Donnelly's work compared to the endurance limit of the fatigued wires within this study can mainly be explained by the smaller grain size and thus an almost polycrystalline microstructure within the struts, despite thinner struts, in Donnelly's study. As a reference, the endurance limit for solution annealed polycrystalline 316LVM with flat geometry was determined by Goebbler [26] at 260 MPa. The stress ratio was chosen with  $R = -1$ , which decreases the endurance limit because of the tension–compression change in each cycle.

The fatigue testing results of the cold drawn oligo-crystalline wires in Figure 4b show significant improvement of the endurance limit to 450 MPa, which is even higher than the endurance limit of the cold worked thick square specimens of Goebbler with an endurance limit of 400 MPa [26]. The cycles to failure decreased strongly for stresses higher than 450 MPa to—in most cases—a few hundred or thousand cycles.

In Figure 5, the elongation of cold drawn and solution annealed wires after fatigue testing is shown. The elongation of the solution-annealed wires is about three times higher than that of the cold drawn for both groups of wires. For the cold drawn state, an elongation of the wires during fatigue testing was only significant for wires where a maximum stress of 450 MPa or higher was applied. Under 450 MPa maximum stress, the cold drawn wires did not exhibit an elongation during fatigue testing. The cyclic creep or “ratchetting” is supported by the positive stress ratio of  $R = 0.5$ , which keeps the wires in tension regime during the entire test. Ratchetting is a directed secondary plastic strain accumulation that can appear additionally during fatigue testing, if the mean stress is higher than zero. The strain accumulation supports a faster development of cracks caused by the fatigue process. Ratchetting of 316L specimens was also reported by Donnelly [16] on struts tested at  $R = 0.1$  and  $R = 0.5$ , respectively, and by Weiß et al. [27], Gaudin et al. [28], Kang et al. [29] and Feaugas et al. [30].



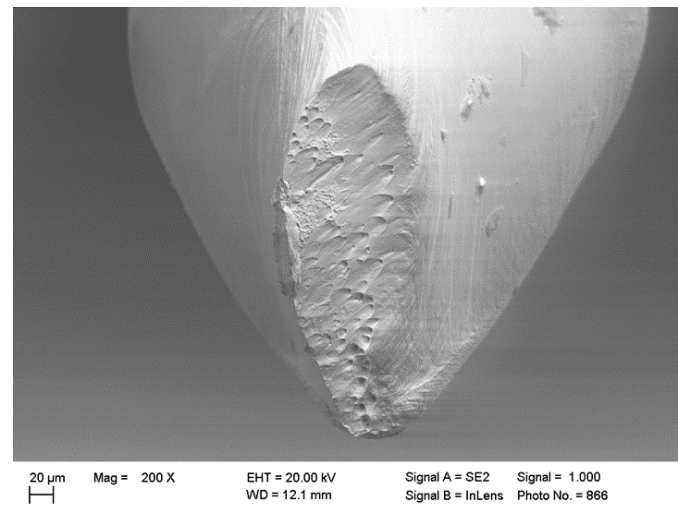
**Figure 5.** Elongation after fatigue testing of fatigue tested wires without rupture and fractured wires.

### 3.3. Microscopy

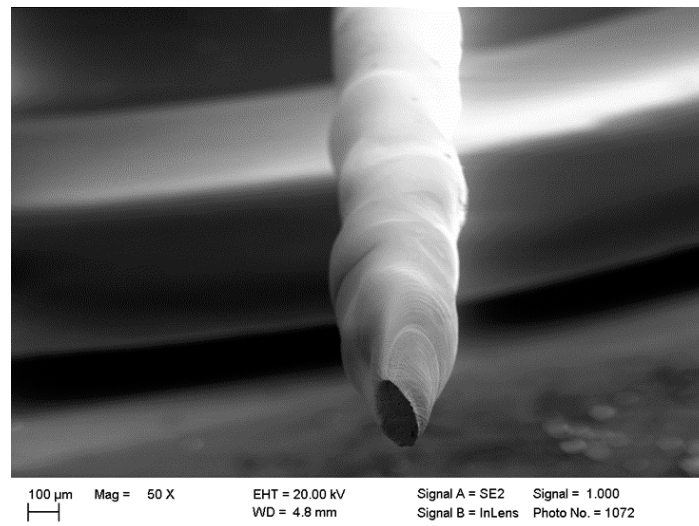
#### 3.3.1. Fractography

Subsequent to the fatigue tests, all wires exhibited regions with high deformation (Figure 6a,b). Slip lines are visible on the entire surface of the wires. Moreover, the wires show a bulge structure as a result of the heavy deformation of the coarse-grained structure.

The wires showed strong lateral contraction and, thus, the fracture surfaces had a small cross-section with respect to the initial diameter of the wire. The slip lines next to the fracture surface were mainly directed to the fracture surface. In regions with pronounced bulging of the wire crossing slip lines due to multiple slip was visible. The fractured surface itself did not look like a conventional fatigue fracture surface with striations or rest lines, but it contained a comparable smooth surface with a blurred honeycomb structure. The ratchetting led to a massive local necking, with the constriction of the wire cross-section during each fatigue cycle. The local stress increased with decreasing cross-sections until geometric softening fracture terminated the fatigue test.



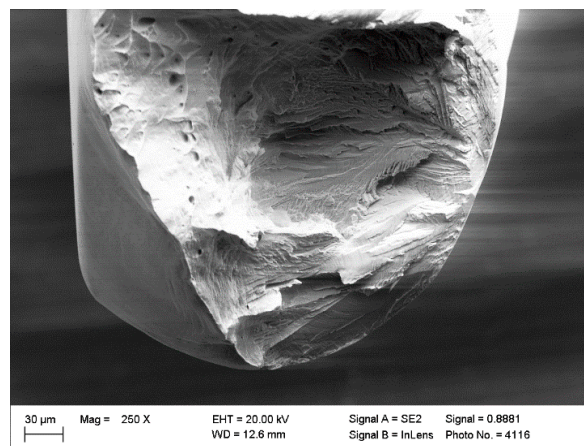
(a)



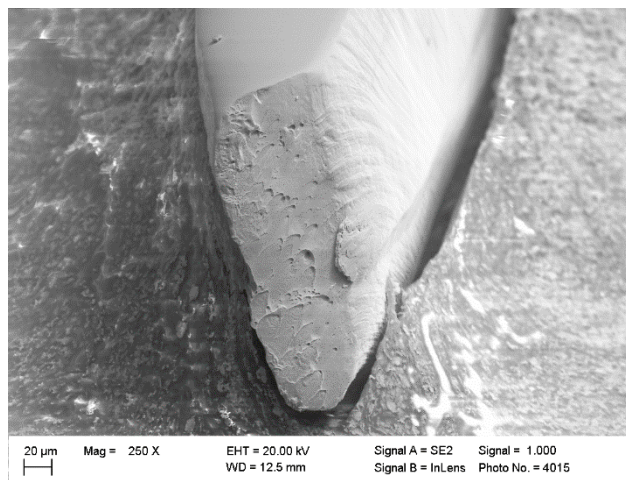
(b)

**Figure 6.** SEM images of (a) a representative fracture surface of an oligo-crystalline wire and (b) overview of the wire surface with bulges after testing (fracture at 1.995 million cycles).

The cold drawn wires exhibited different types of failure, depending on the number of cycles to failure. A typical fatigue fracture surface occurred after failure at 530,000 cycles (Figure 7a), where no pronounced necking was visible. On wires with fractures after, up to, 4000 cycles (Figure 7b), the same type of fracture surface, such as that in the solution annealed wires, was observed. The necking on these wires caused a lateral contraction of the cross section. A smaller cross section led to higher local stresses and, thus, finally, to fracture. Due to grain rotation after cold drawing, the initial diameter (0.5 mm) of the wires was distinctly decreased to 0.374 ( $\pm 0.047$ ) mm. The smallest measured diameter was 0.3 mm, which was approximately a 40% decrease from the initial diameter. Thus, necking was mainly caused by cold drawing in this case. In contrast, necking of the solution annealed wires happened mainly during the cyclic test.



(a)



(b)

**Figure 7.** SEM images of representative fracture surfaces of an oligo-crystalline 10% cold drawn wire after (a) 530,000 cycles and (b) 500 cycles.

### 3.3.2. Electron Backscattering Diffraction

EBSD is used within SEM for the identification of different crystal structures and to determine the orientation of the crystals. EBSD measurements of the solution-annealed wires are shown in Figure 8a–c. The orientation data are represented parallel to the longitudinal direction of the wire. The coloring of the inverse pole figure (IPF) mapping was in accordance with the legend in Figure 8a. The fractured wire in Figure 8 reveals massive grain rotation inside the grain, oriented in the {113} direction, next to the fracture surface. The high deformation became more obvious in the corresponding kernel misorientation mapping (Figure 8b). In general, the kernel misorientation mapping shows low misorientations in blue and increasing misorientations in green and yellow colors. The high kernel average misorientation within the fractured grain in Figure 8 occurs as a result of the strong rotation of the slip planes and the generation of dislocations. The kernel average misorientation (Figure 8b) within this grain is visibly higher than the one in the {111} oriented neighbor grains (blue) in the upper left part of Figure 8a.

Strain hardening, identifiable as micro-twinning, can be seen in the grain boundary mapping (combined with image quality mapping, Figure 8c), wherein the  $\Sigma 3$  twin boundaries have a high density next to the fracture surface. Another representative example of a fractured solution annealed wire, where micro-twinning/hardening is even more pronounced, is shown in Figure 9. In Figures 9a and 9c, massive grain rotations, as well as twinning, are clearly visible.

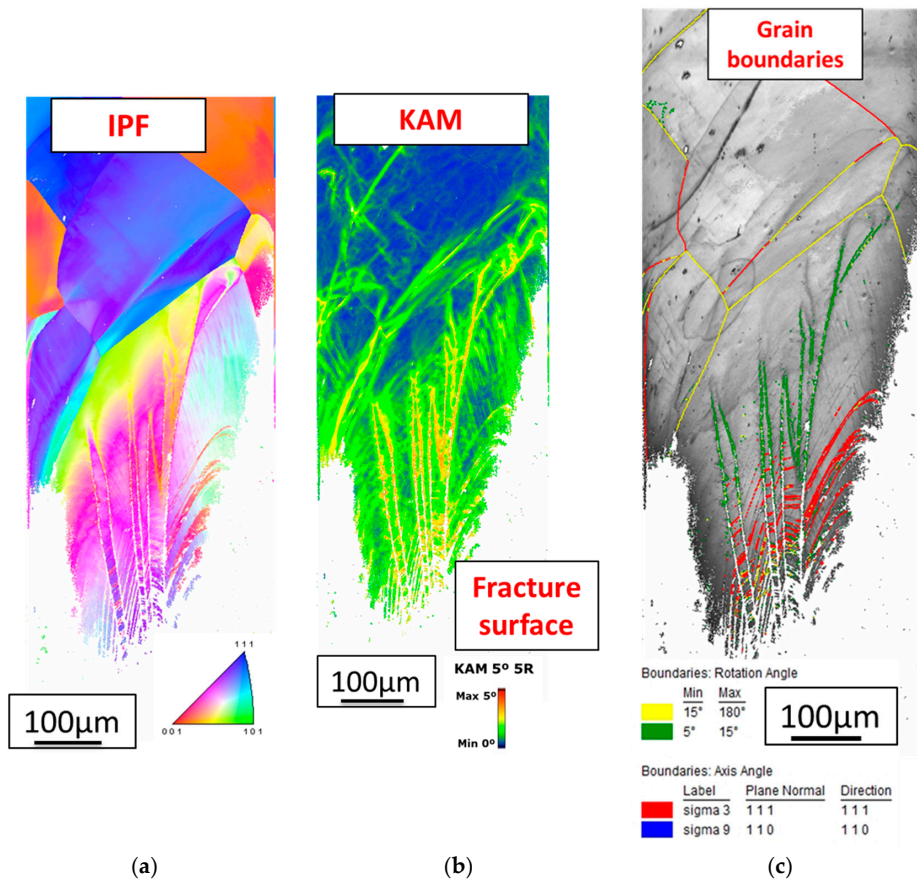


Figure 8. (a) Inverse pole figure mapping, (b) kernel average misorientation (5°5R) mapping, and (c) image quality mapping with grain boundaries of a broken solution annealed oligo-crystalline wire.

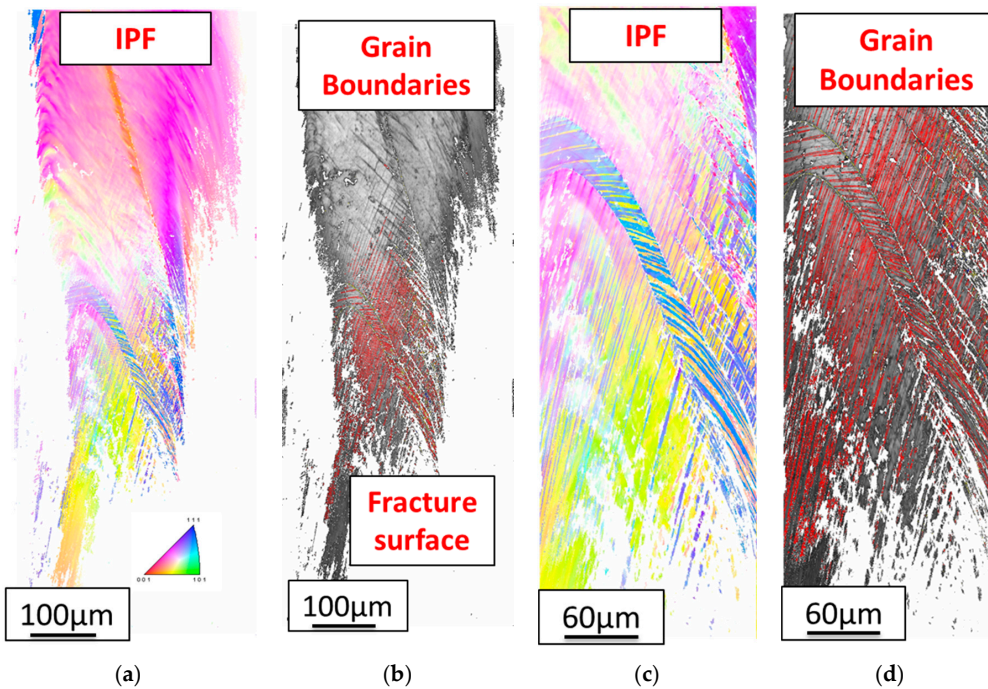
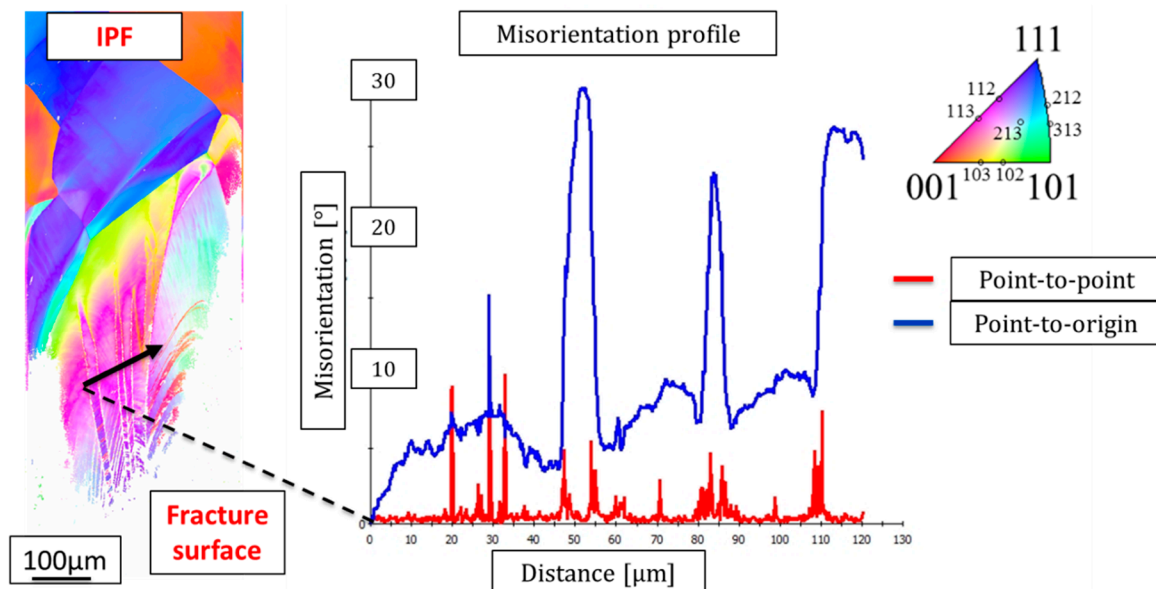


Figure 9. (a) Inverse pole figure mapping (magnification (c)) and (b) image quality mapping with grain boundaries of a broken solution annealed oligo-crystalline wire (magnification (d)).

A closer view to the misorientation profile of the wire (Figure 10) and to the grain boundary mapping in Figure 8c confirms the existence of subgrain boundaries within the strongly-deformed grain, oriented perpendicular to the fracture surface. Such subgrain boundaries can develop due to grain rotation during plastic deformation and subsequent slide along the slip planes, induced by ratchetting/cyclic creep.



**Figure 10.** Inverse pole figure mapping with misorientation profile on subgrain boundaries.

Wires with a {111} and {112} texture (Figure 11a,b, grains colored in violet) show— independent of the wire condition (solution annealed or cold drawn)—no or late fracture. Cold drawing, which is a monotonous strengthening of the material, supports grain rotation into the {111} and {112} direction prior to fatigue, which was also shown by Weiß [17]. Wires with a mixture of near-{111} and {112} oriented grains showed no, or a late, fracture during the fatigue tests compared to wires where, with reference to the inverse pole figure in Figure 12c and Gottstein [31], “middle” oriented, highly deformable grains occur. The fractured grains exhibit a massive grain rotation, which is visualized in the IPF for one example in Figure 12: The crystallographic orientation of these grains shows a “middle” oriented grain and thus a high Schmid factor ( $>0.44$ ), which represents a favorable orientation for slip in relation to the direction of deformation. It is noticeable, that in the fracture grain slip occurs in {113} orientation, which is colored in pink in the IPF mappings. With regards to all analyzed fractured grains, slipping from a “middle” crystallographic orientation into the direction of {113} was observed in 77% of the solution annealed, fractured wires and in 88% of the 10% cold drawn, fractured wires. This observation shows that the mixture of near-{111} and {112} texture is a comparably stable position within an oligo-crystalline microstructure and favorable to withstand fatigue stress and ratchetting.

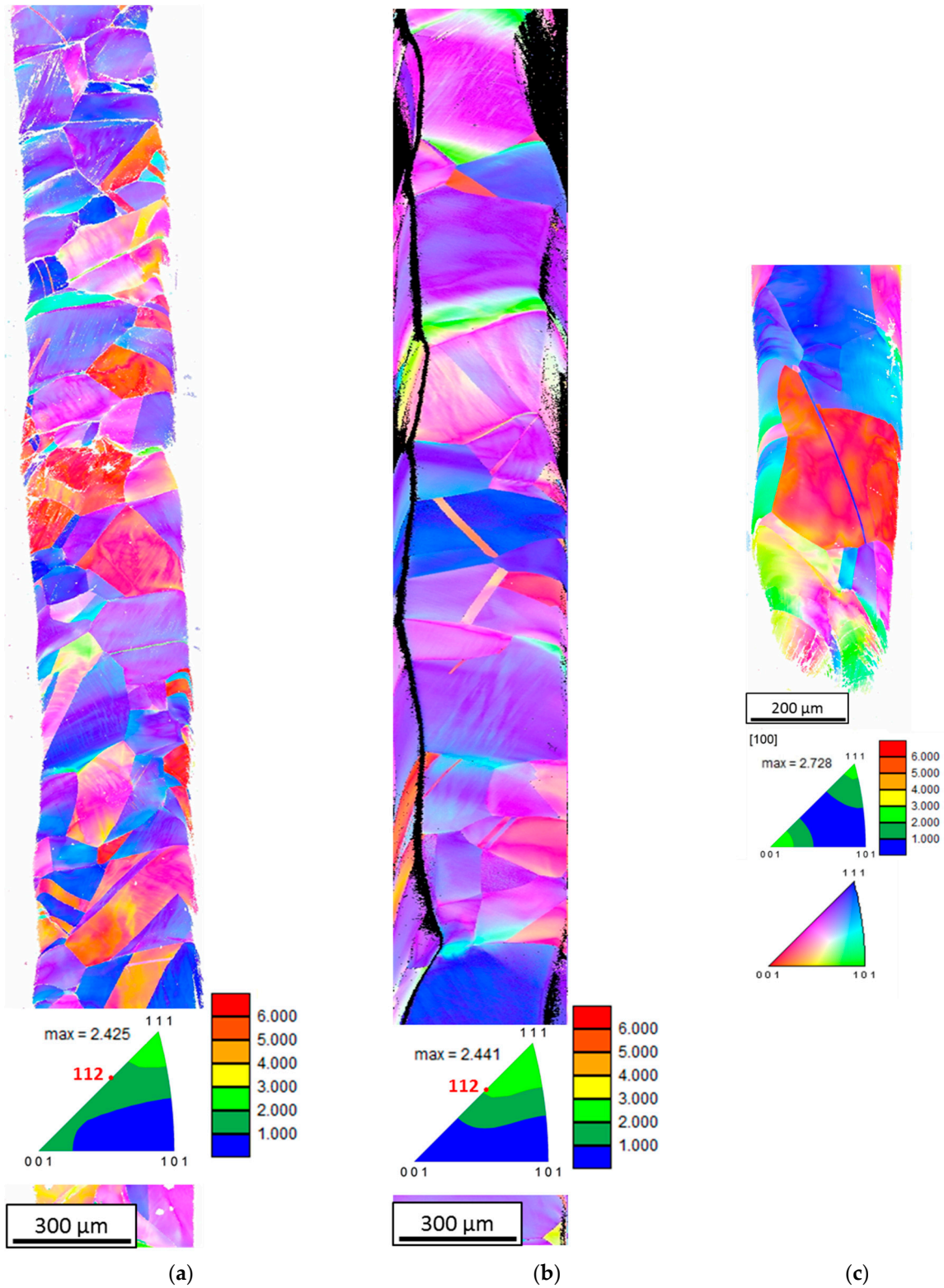


**Figure 11.** Inverse pole figure mappings of (a) solution annealed wire and (b) cold drawn wire (both fatigue tested wires without rupture) and (c) a solution annealed wire with fracture after only 500 cycles.

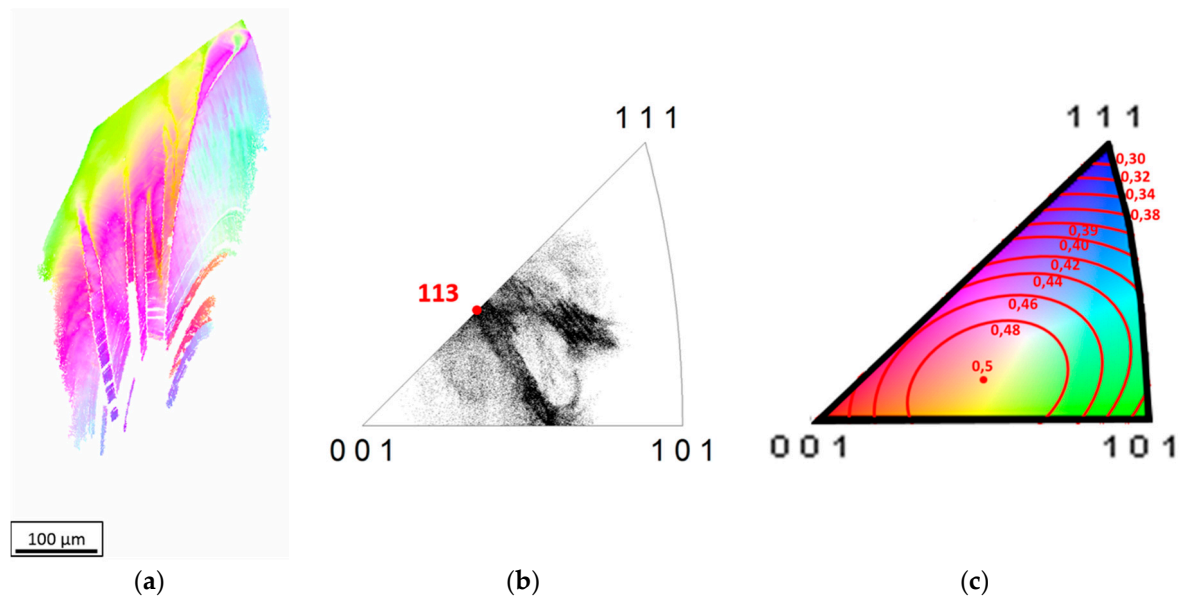


**Figure 12.** (a) IPF | RD mapping of the fractured grain from the solution annealed wire in Figure 8. (b) Inverse pole figures overlapped with the crystallographic orientation of all measured point within the fractured grain and (c) Schmid factor intervals linked with the crystallographic orientation in the inverse pole figure.

#### 4. Conclusions

Within the current study, the properties of oligo-crystalline thin wires in solution annealed, as well as cold drawn state after uniaxial fatigue, were compared. The results give a comprehensive understanding of the influence of cyclic stress on oligo-crystalline microstructures. The following aspects were determined:

- (1) The cold drawing of the oligo-crystalline wires increases the tensile strength from an average of 415 MPa to 804 MPa and decreases the fracture strain from 38% to 8% on average.
- (2) 10% cold drawn oligo-crystalline wires made of 316LVM show a higher endurance limit (450 MPa) than solution annealed ones (250 MPa), due to the generation of a {111} and {112} texture during cold drawing.
- (3) A {111} and {112} texture in oligo-crystalline wires decreases the wire elongation due to ratchetting during fatigue tests at  $R = 0.5$ .
- (4) In addition to the damage induced by cyclic fatigue, all solution annealed wires with less than 4000 cycles to failure exhibit a ratchetting dominated fracture behavior. A bulgy structure is the result of the damaging process. The bulges can lead to lateral contraction and thus to local stress concentration and finally to fracture.
- (5) Fractured wires in 77% of the analyzed oligo-crystalline solution annealed wires and 88% of the 10% cold drawn oligo-crystalline wires exhibited fractured grains with a high Schmid factor ( $>0.44$ ), which showed a rotation to the direction of {113}. Thus, “middle” oriented grains with a high Schmid factor are unfavorable oriented grains for fatigue tests with positive R-ratio.
- (6) Solution annealed oligo-crystalline wires show in average a threefold elongation after end of the test/fracture than cold drawn oligo-crystalline wires.
- (7) Pronounced ratchetting/cyclic creep occurs in fractured wires (elongation after testing is approximately two times higher than that of non-fractured wires).
- (8) Due to grain rotation and wire elongation, cold drawing of the wires can locally decrease the wire diameter up to 40% and cause a bulgy structure with thin wire parts, which has the same appearance as solution annealed wires after ratchetting. Ratchetting is still present, but only at

high stresses over 450 MPa and with less elongation due to the lower strain reserve of cold drawn wires compared to solution annealed wires.

Research on this topic is ongoing. Further results will be published in the near future.

**Acknowledgments:** The authors would like to thank Ing. Alfons Fischer for helpful discussion and the provision of his equipment and Cenk Albayrak for performance of the fatigue tests of the cold drawn wires.

**Conflicts of Interest:** The authors declare no conflict of interest.

## References

1. Kastrati, A.; Mehilli, J.; Dirschinger, J.; Dotzer, F.; Schühlen, H.; Neumann, F.J.; Fleckenstein, M.; Pfafferoth, C.; Seyfarth, M.; Schömig, A. Intracoronary stenting angiographic results: Strut thickness effect on restenosis outcome (ISAR-STEREO) trial. *Circulation* **2001**, *103*, 2816–2821. [[CrossRef](#)] [[PubMed](#)]
2. Perrella, M.; Gerbino, S.; Citarella, R. BEM in Biomechanics: Modelling Advances and Limitations. In *Numerical Methods and Advanced Simulation in Biomechanics and Biological Processes*; Cerrolaza, M., Shefelbine, S.J., Garzon-Alvarado, D., Eds.; Academic Press: Cambridge, MA, USA, 2017; ISBN 9780128117187.
3. Li, Y.; Laird, C. Cyclic response and dislocation structures of AISI 316L stainless steel. Part 1: Single crystals fatigued at intermediate strain amplitude. *Mater. Sci. Eng. A* **1994**, *186*, 65. [[CrossRef](#)]
4. Li, Y.; Laird, C. Cyclic response and dislocation structures of AISI 316L stainless steel. Part 2: Polycrystals fatigued at intermediate strain amplitude. *Mater. Sci. Eng. A* **1994**, *186*, 87. [[CrossRef](#)]
5. Pache, J.; Kastrati, A.; Mehilli, J.; Schühlen, H.; Dotzer, F.; Örg Hausleiter, J.; Fleckenstein, M.; Neumann, F.J.; Sattelberger, U.; Schmitt, C.; et al. Intracoronary stenting angiographic results: Strut thickness effect on restenosis outcome (ISAR-STEREO-2) trial. *J. Am. Coll. Cardiol.* **2003**, *41*, 1283–1288. [[CrossRef](#)]
6. Briguori, C.; Sarais, C.; Pagnotta, P.; Liistro, F.; Montorfano, M.; Chieffo, A.; Sgura, F.; Corvaja, N.; Albiero, R.; Stankovic, G.; et al. In-stent restenosis in small coronary arteries: Impact of strut thickness. *J. Am. Coll. Cardiol.* **2002**, *40*, 403–409. [[CrossRef](#)]
7. Rittersma, S.Z.H.; de Winter, R.J.; Koch, K.T.; Bax, M.; Schotborgh, C.E.; Mulder, K.J.; Tijssen, J.G.P.; Piek, J.J. Impact of Strut Thickness on Late Luminal Loss After Coronary Artery Stent Placement. *Am. J. Cardiol.* **2004**, *93*, 477–480. [[CrossRef](#)] [[PubMed](#)]
8. Kitabata, H.; Kubo, T.; Komukai, K.; Ishibashi, K.; Tanimoto, T.; Ino, Y.; Takarada, S.; Ozaki, Y.; Kashiwagi, M.; Orii, M.; et al. Effect of strut thickness on neointimal atherosclerotic change over an extended follow-up period ( $\geq 4$  years) after bare-metal stent implantation: Intracoronary optical coherence tomography examination. *Am. Heart J.* **2012**, *163*, 608–616. [[CrossRef](#)] [[PubMed](#)]
9. Stolpmann, J.; Brauer, H.; Stracke, H.J.; Erbel, R.; Fischer, A. Practicability and Limitations of Finite Element Simulation of the Dilatation Behavior of Coronary Stents. *Materialwissenschaft und Werkstofftechnik* **2003**, *34*, 736–745. [[CrossRef](#)]
10. Murphy, B.P.; Savage, P.; McHugh, P.E.; Quinn, D.F. The stress-strain behavior of coronary stent struts is size dependent. *Ann. Biomed. Eng.* **2003**, *31*, 686–691. [[CrossRef](#)] [[PubMed](#)]
11. Weiß, S.; Schnauber, T.; Fischer, A. Microstructure Characterization of thin structures after deformation. In Proceedings of the Materials and Devices for Smart Systems III, Boston, MA, USA, 1–4 December 2008; pp. 349–354.
12. Mitevski, B.; Fischer, A.; Weiß, S. In Situ Tensile Testing of Notched Poly- and Oligocrystalline 316L Wires. *Mater. Test.* **2014**, *59*, 130–135. [[CrossRef](#)]
13. Wimmer, A.; Leitner, A.; Detzel, T.; Robl, W.; Heinz, W.; Pippan, R.; Dehm, G. Damage evolution during cyclic tension-tension loading of micron-sized Cu lines. *Acta Mater.* **2014**, *67*, 297–307. [[CrossRef](#)]
14. Wiersma, S.; Taylor, D. Fatigue of materials used in microscopic components. *Fatigue Fract. Eng. Mater. Struct.* **2005**, *28*, 1153–1160. [[CrossRef](#)]
15. Meißner, A. Mechanische Eigenschaften Wenigkristalliner Strukturen. Ph.D. Thesis, University of Duisburg-Essen, Duisburg, Germany, 2006.
16. Donnelly, E. Geometry Effect in the Fatigue Behaviour of Microscale 316L Stainless Steel Specimens. Ph.D. Thesis, National University of Ireland, Galway, Ireland, 2012.
17. Weiß, S. Einfluss der Wenigkristallinität auf das Verformungsverhalten von Werkstoffen und Bauteilen der Medizintechnik. Habilitation Thesis, University of Duisburg-Essen, Duisburg, Germany, 2008.

18. Hsiao, Z.W.; Wu, T.Y.; Chen, D.; Kuo, J.C.; Lin, D.Y. EBSD and electron channeling study of anomalous slip in oligocrystals of high chromium ferritic stainless steel. *Micron* **2017**, *94*, 15–25. [[CrossRef](#)] [[PubMed](#)]
19. Lim, H.; Carroll, J.D.; Battaile, C.C.; Boyce, B.L.; Weinberger, C.R. Quantitative comparison between experimental measurements and CP-FEM predictions of plastic deformation in a tantalum oligocrystal. *Int. J. Mech. Sci.* **2015**, *92*, 98–108. [[CrossRef](#)]
20. Lim, H.; Carroll, J.D.; Battaile, C.C.; Buchheit, T.E.; Boyce, B.L.; Weinberger, C.R. Grain-scale experimental validation of crystal plasticity finite element simulations of tantalum oligocrystals. *Int. J. Plast.* **2014**, *60*, 1–18. [[CrossRef](#)]
21. Chen, B.; Jiang, J.; Dunne, F.P.E. Microstructurally-sensitive fatigue crack nucleation in Ni-based single and oligo crystals. *J. Mech. Phys. Solids* **2017**, *106*, 15–33. [[CrossRef](#)]
22. Guan, Y.; Chen, B.; Zou, J.; Britton, B.; Jiang, J.; Dunne, F.P.E. Crystal plasticity modelling and HR-DIC measurement of slip activation and strain localization in single and oligo-crystal Ni alloys under fatigue. *Int. J. Plast.* **2017**, *88*, 70–88. [[CrossRef](#)]
23. Klusemann, B.; Svendsen, B.; Vehoff, H. Modeling and simulation of deformation behavior, orientation gradient development and heterogeneous hardening in thin sheets with coarse texture. *Int. J. Plast.* **2013**, *50*, 109–126. [[CrossRef](#)]
24. Henning, M.; Vehoff, H. Local mechanical behavior and slip band formation within grains of thin sheets. *Acta Mater.* **2005**, *53*, 1285–1292. [[CrossRef](#)]
25. Cuddihy, M.A.; Stapleton, A.; Williams, S.; Dunne, F.P.E. On cold dwell facet fatigue in titanium alloy aero-engine components. *Int. J. Fatigue* **2017**, *97*, 177–189. [[CrossRef](#)]
26. Gobbeler, P. *Untersuchungen zum Ermüdungsverhalten des kalt Umgeformten Austenitischen Implantatwerkstoffs X2CrNiMo18-15-3*; Diss. Universität Essen, VDI Fortschrittberichte, Reihe 5 Grund-und Werkstoffe Nr. 513; VDI Verlag: Düsseldorf, Germany, 1998.
27. Weiß, E.; Postberg, B.; Nicak, T.; Rudolph, J. Simulation of ratchetting and low cycle fatigue. *Int. J. Pres. Ves Pip.* **2004**, *81*, 235–242. [[CrossRef](#)]
28. Gaudin, C.; Feaugas, X. Cyclic creep process in AISI 316L stainless steel in terms of dislocation patterns and internal stresses. *Acta Mater.* **2003**, *52*, 3097–3110. [[CrossRef](#)]
29. Kang, G.Z.; Li, Y.G.; Zhang, J.; Sun, Y.F.; Gao, Q. Uniaxial ratchetting and failure behaviour of two steels. *Theor. Appl. Fract. Mech.* **2004**, *43*, 199–209. [[CrossRef](#)]
30. Feaugas, X.; Gaudin, C. Ratchetting process in the stainless steel AISI 316L at 300K: An experimental investigation. *Int. J. Plast.* **2003**, *20*, 643–662. [[CrossRef](#)]
31. Gottstein, G. *Physikalische Grundlagen der Materialkunde*; Springer: Berlin, Germany, 1998.



© 2018 by the authors. Licensee MDPI, Basel, Switzerland. This article is an open access article distributed under the terms and conditions of the Creative Commons Attribution (CC BY) license (<http://creativecommons.org/licenses/by/4.0/>).